ELSEVIER

Solid State Ionics 48 (2002) 71–81

SOLID STATE IONICS

www.elsevier.com/locate/ssi

Synthesis and hydrogen permeation properties of membranes based on dense $SrCe_{0.95}Yb_{0.05}O_{3-\alpha}$ thin films

Satoshi Hamakawa[1], Lin Li, Anwu Li, Enrique Iglesia*

Department of Chemical Engineering, University of California at Berkeley, Berkeley, CA 94720-1462, USA
Division of Materials Sciences, E.O. Lawrence Berkeley National Laboratory, Berkeley, CA 94720, USA

Received 3 October 2001; received in revised form 18 December 2001; accepted 20 December 2001

Abstract

Dense $SrZr_{0.95}Y_{0.05}O_{3-\alpha}$ and $SrCe_{0.95}Yb_{0.05}O_{3-\alpha}$ thin films with perovskite structure were prepared on porous $SrZr_{0.95}Y_{0.05}O_{3-\alpha}$ substrates by spin coating colloidal suspensions of powders prepared by combustion methods. Porous substrates were prepared by treating carbon/$SrZr_{0.95}Y_{0.05}O_{3-\alpha}$ composites in air at 1273–1573 K in order to combust the carbon and partially sinter the resulting porous oxide. This procedure led to strong porous solids with a high gas permeability. Matching the shrinkage of the porous substrate and of the thin film by this pre-sintering of the porous substrate led to thin films free of fissures and other defects. Thin films prepared by these methods did not transport He at ambient temperature or N_2 at 900–1000 K. H_2 permeation rates through $SrCe_{0.95}Yb_{0.05}O_{3-\alpha}$ thin films at 950 K were as high as 500 times larger than on 1-mm disks and reached values of 6×10^{-4} mol H_2/cm^2 min for 2 μm films. H_2 permeation rates were proportional to the inverse of the membrane thickness, indicating that permeation in $SrCe_{0.95}Yb_{0.05}O_{3-\alpha}$ thin films is controlled by bulk diffusion and not by H_2 dissociative chemisorption or by boundary layer transport, even for 2 μm films.

Keywords: $SrCe_{0.95}Yb_{0.05}O_{3-\alpha}$; Hydrogen permeation; Thin films

1. Introduction

High-temperature proton conductors based on mixed oxides with perovskite structures have attracted considerable attention. Early studies focused on exploratory development of new compositions and on their characterization by total conductivity measurements in various environments [1–5]. More recent reports have included hydrogen permeation measurements, which are critical in order to assess the function of these materials as hydrogen-permeable membranes [6,7]. Proton conduction through dense solids involves migration through the crystalline oxide lattice. Selective H_2 permeation requires a low diffusivity of lattice oxygen, which is normally associated with electronic insulators [8] that cannot be used for proton transport in open circuit modes because of the additional requirement for electron or hole conduction through the solid. The requirement of low oxygen conductivity also requires that proton conduction occur at practical rates at relatively low temperatures (<1100 K).

Significant advances in the proton conductivity have been brought forth by the development of doped

* Corresponding author. Department of Chemical Engineering, University of California at Berkeley, Berkeley, CA 94720-1462, USA. Fax: +1-510-642-4778.

E-mail address: iglesia@cchem.berkeley.edu (E. Iglesia).

[1] Permanent address: National Institute of Advanced Industrial Science and Technology, 1-1 Higashi, Tsukuba, Ibaraki 305-8565, Japan.

0167-2738/02/$ - see front matter
PII: S0167-2738(02)00047-4

perovskite structures, but permeation rates remain unattractive for non-electrochemical removal of H_2 from dilute streams. Typically, these materials are used as 1–2 mm thick disks or as tubes with thick walls (>2 mm). Permeation rates are inversely proportional to the thickness of the membrane when permeation across the membrane is controlled by transport through the solid phase and not by boundary layer transport or by the activation of H_2 at membrane surfaces. Therefore, membranes consisting of dense films supported on porous substrates should lead to much higher permeation rates than the larger structures currently used. Several methods have been used for the synthesis of ion-conducting oxides as thin films, but most previous studies focused on structural characterization or conductivity measurements, without detailed measurements of permeation rates.

Itoh et al. [9] prepared $Ca(Ti,Fe)O_3$ thin films by spin-coating $Ca(Ti,Fe)O_3$ powders dispersed in isopropanol onto $CaTiO_3$ porous substrates, and subsequently treating these composites at 1473–1573 K in air for 2 h to form 20–50 μm thin films impermeable to N_2. The O_2 permeation rates of $1–6 \times 10^{-7}$ mol/cm^2 min at 1273 K were significantly higher than for disks of identical composition. Visco et al. [10] coated NiO–YSZ substrates with colloidal suspensions of yttria-stabilized zirconia (YSZ) powders prepared by glycine–nitrate methods. Dense YSZ thin films (4–10 μm) were obtained after treatment in air at 1673 K for 1 h. Fissures and cracks were minimized by partial shrinkage of a nonporous mechanical support in order to match its subsequent shrinkage with that of the coated powders. The NiO-based supports were nonporous during film deposition, but became porous (and electrically conducting) by subsequent reduction of the NiO. Eschenbaum et al. [11] prepared $SrZr_{0.95}Yb_{0.05}O_{3-\alpha}$ thin films on nonporous silicon substrates by depositing a precursor formed via sol–gel methods, treating the composites in air at 873 K in order to remove organic residues, and then sintering at 973–1273 K. X-ray diffraction measurements detected crystalline $SrZrO_3$. Scanning electron micrographs revealed highly irregular defective films with a high density of fissures. Kosaki and Anderson [12] prepared $SrCe_{0.95}Yb_{0.05}O_{3-\alpha}$ thin films with perovskite structure (~ 1 μm) on dense silicon or Al_2O_3 substrates using a polymer precursor method. Only the structure and electrical conductivity of the films were reported. The higher total conductivity of the films compared with dense polycrystalline $SrCe_{0.95}Yb_{0.05}O_{3-\alpha}$ disks was attributed to smaller grains in the thin films than in the larger dense structures.

Here, we describe procedures for the synthesis of nonporous $SrZr_{0.95}Y_{0.05}O_{3-\alpha}$ and $SrCe_{0.95}Yb_{0.05}O_{3-\alpha}$ thin films prepared on porous substrates by spin coating colloidal suspensions of powders prepared by combustion methods. We also describe methods for the synthesis and partial sintering of perovskite substrates with high porosity and for the deposition and densification of thins films. The structure and H_2 permeation properties of these dense films were determined by scanning electron microscopy and high-temperature permeation measurements, respectively. Films with 2–140 μm thickness led to H_2 permeation rates up to 500 times greater than for 1 mm disks of identical composition.

2. Experimental

2.1. Synthesis of dense films and disks and of porous supports

Combustion methods were used in order to prepare $SrZr_{0.95}Y_{0.05}O_{3-\alpha}$ and $SrCe_{0.95}Yb_{0.05}O_{3-\alpha}$ precursor powders. Glycolic acid and citric acid were used as complexing agents and fuels for the synthesis of $SrZr_{0.95}Y_{0.05}O_{3-\alpha}$ and $SrCe_{0.95}Yb_{0.05}O_{3-\alpha}$ powders, respectively. The powders were treated in ambient air at 0.0825 K/s to 1273 K for 2 h. X-ray diffraction detected the expected perovskite structures in all powders. Detailed synthesis procedures have been reported previously [13,14]. A dense $SrCe_{0.95}Yb_{0.05}O_{3-\alpha}$ disk (1 mm thickness) was prepared by treating powders compacted at ~ 120 MPa in a 2.5 cm die for 10 h at 1873 K in ambient air.

Porous disks with $SrZr_{0.95}Y_{0.05}O_{3-\alpha}$ composition and perovskite structure were used to support dense films of both $SrZr_{0.95}Y_{0.05}O_{3-\alpha}$ and $SrCe_{0.95}Yb_{0.05}O_{3-\alpha}$. These porous substrates showed good mechanical integrity and stability in both oxidizing and reducing environments. They remained porous even after treatment at 1873 K in ambient air, a procedure required in order to densify the perovskite powders coated onto their surfaces into dense films. These films and substrates remained intact in H_2 (1 bar) at 1073 K. Porous substrates were prepared by ultra-

sonically dispersing $SrZr_{0.95}Y_{0.05}O_{3-\alpha}$ powders and carbon black (Fisher) in isopropanol for 0.5–1.0 h. The slurry was filtered, dried in ambient air at ~ 300 K, and then the $SrZr_{0.95}Y_{0.05}O_{3-\alpha}$ powders (1.6 g) were compacted at ~ 120 MPa using a 2.5 cm die. These disks were partially sintered in ambient air and the carbon black combusted by heating in flowing ambient air at a slow ramping rate (0.033 K/s) in order to avoid cracking. The carbon black content and the sintering temperature of the carbon-perovskite composites were varied in order to determine conditions that accurately matched the shrinkage profile of the porous substrates with that of the deposited perovskite films during the final sintering of the composite membrane, as discussed in detail below.

The synthesis of thin films involved grinding of oxide powders ($SrZr_{0.95}Y_{0.05}O_{3-\alpha}$ or $SrCe_{0.95}Yb_{0.05}O_{3-\alpha}$, 2–5 wt.%) in a mortar and pestle for 30 min and ultrasonically dispersing these powders as an isopropanol slurry for 1 h in order to break up loose agglomerates and to form a homogeneous dispersion. About 1 cm^3 of the colloidal dispersion was added dropwise onto a pre-sintered porous substrate as the porous substrate rotated at 30–50 Hz. After each coating step, the sample was dried in ambient air at room temperature for 1 h. After three coatings, the membrane was partially sintered in ambient air at the same heating rate and final pre-sintering temperature and time used for the synthesis of the substrate. This was done in order to prevent the development of cumulative stresses during sequential coating steps. The coating–drying–sintering cycles, which can be used to deposit ~ 2 μm films during each cycle, were repeated several times in order to vary the film thickness. After coating, the film–substrate composite was treated in Ar (7 kPa) by increasing the temperature to 1873 K at 0.033 K/s and holding for 2 h. The composite was cooled to ambient temperature at a slow rate (0.067 K/s) in order to prevent thermal stresses, which tend to develop during rapid or nonuniform cooling. The samples were then treated at 1273 K for 2 h in ambient air in order to replace any lattice oxygen atoms removed during the Ar treatment and to restore the stoichiometric perovskite composition. The synthesis procedure is shown schematically in Fig. 1.

2.2. Characterization of the structure and permeation properties of thin films and porous substrates

The permeability of the porous substrates and the integrity of the dense films were examined at ambient temperature by sealing the edges of the substrates and

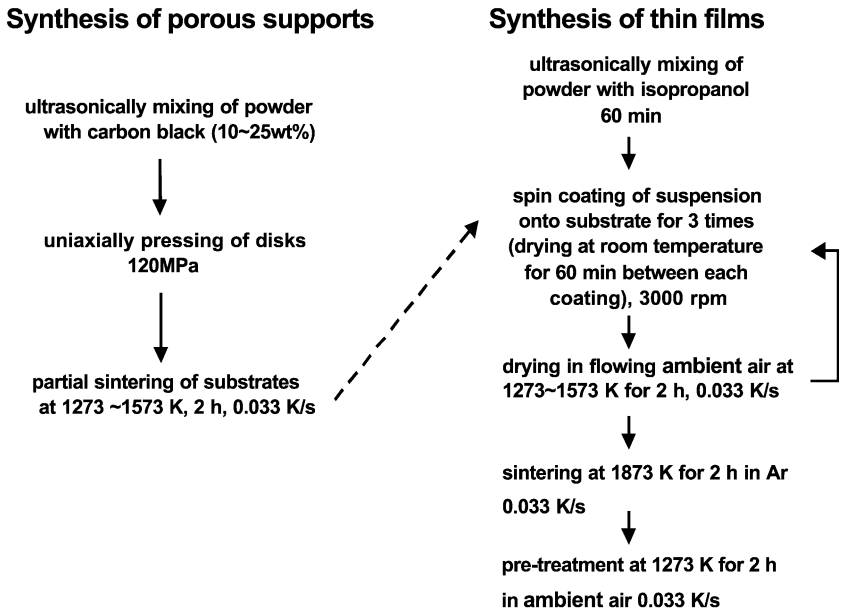

Fig. 1. Procedures for the synthesis of porous substrates and thin films.

composites using O-rings and a silicone sealant. Helium permeation rates through either the porous substrates, to measure their permeability, or through the composites, to confirm their dense nature, were obtained using a bubble meter at various pressure differences across the materials (50–350 kPa). The shrinkage rates of these porous substrates were determined by measuring the diameter of the disk before and after thermal treatments. A dual-stage ISI-DS130C scanning electron microscope (SEM) was used to examine the morphology of the substrates and the composites, as well as the thickness of the top layer. The perovskite structure was confirmed by X-ray diffraction using a Siemens Diffractometer D5000 and Cu Kα radiation.

The H_2 flux through $SrCe_{0.95}Yb_{0.05}O_{3-\alpha}$ films was measured using a high-temperature permeation apparatus. Gas flow rates were metered using electronic mass flow controllers in both sides of the membrane (Porter). The membrane disk was held between two alumina tubes and sealed with a glass ring that softens at 873 K. One side of the membrane (upstream) was exposed to H_2 (99.99%) diluted to the desired concentration using He (99.999%) or N_2 (99.999%). The other side (downstream) was swept with N_2/O_2 and He, as a sweep gas. The flow rates of upstream and downstream gases were 50 and 60 cm^3/min, respectively. When the permeate side was swept with He or N_2, a make-up O_2 stream (10 ml/min) was introduced downstream of the membrane module and of the mass spectrometer sampling point in order to convert H_2 to water using a Pt mesh (Alfa Aesar, 100 mesh) at 973 K. H_2 permeation rates through the membrane were measured using a mass spectrometer (Transpector, Leybold-Inficon) to analyze the permeate stream and confirmed by a humidity meter (HMI 38, Vaisala).

3. Results and discussions

3.1. Synthesis of porous substrates

The synthesis variables that influence the porosity and permeability of the porous substrates were systematically examined in order to obtain strong and stable substrates and to match their shrinkage profiles with those of the dense top layer. These variables included the carbon content in the composites, the temperature of the thermal treatment in ambient air, and the pressure used in order to compact the perovskite–carbon composite.

The amount of carbon, the time held at the maximum sintering temperature, and the heating rate influenced the permeability of the porous support. Fig. 2 shows the results of permeation measurements at ambient temperature on porous substrates obtained by varying these three variables. These substrates were prepared as described in Section 2.2, but sintered to 1873 K in order to simulate the treatment that would be ultimately required to form thin films from powders coated on their surfaces. The permeability of the porous substrate increased as the amount of carbon black (Fig. 2a) or the heating rate increased (Fig. 2c). It decreased with increasing holding time at the maximum temperature (Fig. 2b).

The porosity of these substrates arises from voids created by the combustion of carbon black. Therefore, higher carbon black concentrations lead to larger void fractions in $SrZr_{0.95}Y_{0.05}O_{3-\alpha}$ substrate and to higher permeation rates. The heating rate and the time held at the highest sintering temperature also influence the extent of densification; the pore volume and the average pore size decrease as densification occurs. The temperature at which powder precursors were treated before pressing into disks and the extent of mixing between $SrZr_{0.95}Y_{0.05}O_{3-\alpha}$ and carbon black (with or without ultrasonic mixing) also influenced porosity and permeation rates. Higher treatment temperatures before pressing increased the particle size of the oxide component, which led to larger voids between perovskite crystallites and to slower densification. The elimination of the ultrasonic dispersion step led to larger pores because the composite material contained much larger carbon and oxide agglomerates. The flexibility introduced by the systematic control of these variables confirmed that porous substrates with a wide range of morphologies, permeation rates, and mechanical strength can be prepared in order to match the densification requirements of films with a wide compositional range.

The initial partial sintering of the substrate before film deposition is required in order to (1) ensure the formation of solid bridges between the particles, required for structural integrity and mechanical strength, (2) decompose the carbon black precursors and form the required voids, and (3) match the shrinkage of the

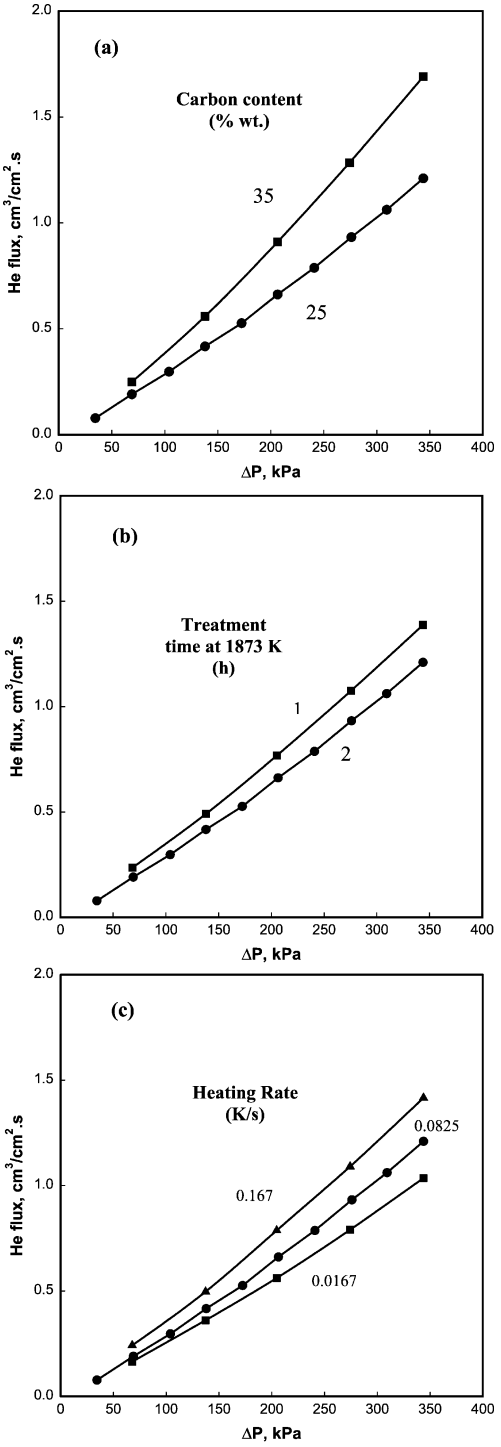

substrate to that of the thin film. Substrates partially sintered above 1273 K were sufficiently strong for spin coating procedures. The combustion of the carbon black must occur before deposition of thin films in order to avoid the significant temperature gradients and the rapid gas evolution caused by this combustion step, which can lead to nonuniform densification of the films and to the formation of fissures or defects. Temperature-programmed oxidation studies showed that the carbon component mixed with $SrZr_{0.95}Y_{0.05}O_{3-\alpha}$ oxidizes to CO_2 at $\sim$ 970 K. Thus, pre-sintering in air at 1273 K is sufficient to achieve the required strength and to create the porosity resulting from the combustion of the carbon component.

Large differences between the densification rates of the thin films and of the porous substrates lead to fissures and defects, which were easily detected by optical microscopy and by high He permeation rates at ambient temperature through the film–substrate composites. Fig. 3 shows that significant densification of the porous substrate (34% vol.) occurs between 1473 and 1873 K. Thin films deposited on this porous substrate must shrink to similar extents when treated at 1873 K in order to form dense and defect-free thin films with good adherence to the porous substrate. There is no method to measure directly and during synthesis the shrinkage rate of the thin films in order to accurately match that of the substrate as it is heated from the pre-sintering temperature (1273 K) to the final temperature required to form dense films (1873 K). The relative shrinkage rates of the thin films and the substrates can be inferred after sintering, however, by inspection of the curvature of the film–substrate composites. Concave film surfaces indicate that the thin film densified faster than the porous substrate, while a convex film surface reflects the faster densification of the porous substrate. The pre-sintering of the porous $SrZr_{0.95}Y_{0.05}O_{3-\alpha}$ substrates at 1273–1573 K before film deposition slows down the subsequent densification of these substrates during subsequent treatment of

Fig. 2. Helium flux through porous substrates at ambient temperature as a function of the pressure difference across the disk. Permeate side at ambient pressure. (a) Effect of carbon black content, heating rate: 0.0167 K/s to 1873 K, holding time 2 h. (b) Effect of holding time at 1873 K, carbon black: 25 wt.%, heating rate: 0.0167 K/s. (c) Effect of the heating rate to 1873 K, carbon black: 25 wt.%, 2-h holding time at 1873 K.

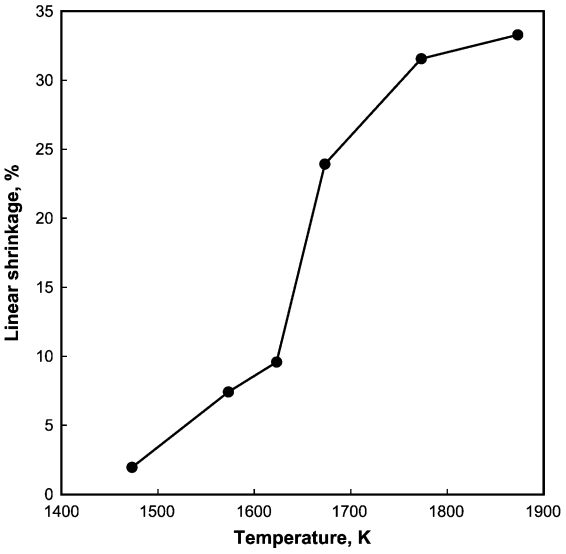

Fig. 3. Effect of sintering temperature on the shrinkage of porous substrates. Carbon black: 25 wt.%, heating rate: 0.0825 K/s, 2 h holding time at final temperature.

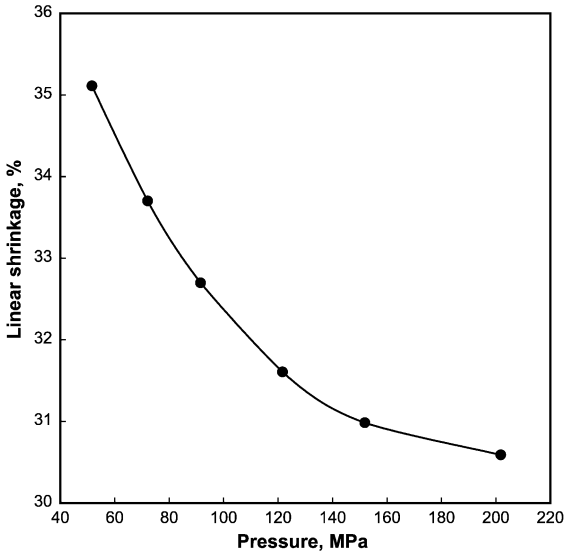

Fig. 4. Effect of compaction pressure on the shrinkage of porous substrates. Carbon black: 25 wt.%, heating rate: 0.0825 K/s, 2 h holding time at 1873 K.

the film–substrate composites at 1873 K and leads to the coincident shrinkage of the two layers and to flat film–substrate composites.

The extent of densification of the porous substrate can also be controlled by varying the compaction pressure used to form the carbon–perovskite precursors. Fig. 4 shows that the extent of densification after treatment at 1873 K in air for 2 h decreased from 35% to 30% as the compaction pressure increased from 50 to 200 MPa. These effects are small compared with those achieved by varying the pre-sintering temperature. Therefore, compaction pressures were used only to fine-tune the density of the porous substrates before film deposition. This compaction pressure influences the initial void volume of carbon-containing disks which leads to variations in the residual void volume after sintering. As reported previously, more extensive compaction of the perovskite–carbon composite leads to smaller losses in pore volume during subsequent thermal treatment [14].

3.2. Synthesis and structure of thin films supported on porous substrates

Based on the densification behavior of the porous substrates and the films, $SrZr_{0.95}Y_{0.05}O_{3-\alpha}$ and $SrCe_{0.95}Yb_{0.05}O_{3-\alpha}$ thin films were successfully prepared by spin coating powders synthesized via combustion methods onto pre-sintered porous substrates. $SrZr_{0.95}Y_{0.05}O_{3-\alpha}$ powders were used to prepare the porous substrates for both film compositions, because $SrCe_{0.95}Yb_{0.05}O_{3-\alpha}$ formed much weaker porous disks. Substrate synthesis and treatment conditions must be tailored for each film layer material in order to match the shrinkage characteristics of the corresponding film. Table 1 shows the procedures used for the synthesis of the porous substrates in each case. For $SrCe_{0.95}Yb_{0.05}O_{3-\alpha}$ films, lower carbon contents and higher pre-sintering temperatures were required,

Table 1
Synthesis procedures for $SrZr_{0.95}Y_{0.05}O_{3-\alpha}$ porous substrates used as film supports

Composition of film	$SrZr_{0.95}Y_{0.05}O_{3-\alpha}$	$SrCe_{0.95}Yb_{0.05}O_{3-\alpha}$
Carbon black (wt.%)	25	10 or 20
Pressing pressure (MPa)	120	120
Pre-sintering protocols	0.0167 K/s to 1273 K in flowing ambient air and 2-h hold	0.033 K/s to 1573 K in flowing ambient air and 2-h hold

because the shrinkage for $SrCe_{0.95}Yb_{0.05}O_{3-\alpha}$ films was significantly less than for $SrZr_{0.95}Y_{0.05}O_{3-\alpha}$ films.

Scanning electron micrographs of representative $SrZr_{0.95}Y_{0.05}O_{3-\alpha}$ thin films on porous substrates are shown in Fig. 5. The micrograph shown in Fig. 5 is that of a 20 μm film prepared by nine coatings of $SrZr_{0.95}Y_{0.05}O_{3-\alpha}$ (Table 2). This film shows excellent adhesion to the substrate and no detectable porosity or surface imperfections. Room temperature permeation tests showed that this material was impermeable to He at ambient temperature and 200 kPa. The successful synthesis of nonporous thin films by partial sintering of porous substrates suggests that the spin coating procedures used were able to deposit powder precursors uniformly on the porous substrate surfaces.

Dense top layers of $SrCe_{0.95}Yb_{0.05}O_{3-\alpha}$ (80–140 μm) prepared by the method described in Table 2 are evident from the micrographs in Fig. 6b,c. The structure of the film in Fig. 6a differed from those in the other two samples shown. The total thickness of the $SrCe_{0.95}Yb_{0.05}O_{3-\alpha}$ top layer was about 20 μm, but all but the lowest 2 μm showed a structure with large pores, with a dense 2 μm film at the interface between the $SrCe_{0.95}Yb_{0.05}O_{3-\alpha}$ top layer and the $SrZr_{0.95}Y_{0.05}O_{3-\alpha}$ porous substrate. Thus, the perme-

Table 2
Preparation conditions for $SrZr_{0.95}Y_{0.05}O_{3-\alpha}$ and for $SrCe_{0.95}Yb_{0.05}O_{3-\alpha}$ films on $SrZr_{0.95}Y_{0.05}O_{3-\alpha}$ porous substrates

Top layer	$SrZr_{0.95}Y_{0.05}O_{3-\alpha}$	$SrCe_{0.95}Yb_{0.05}O_{3-\alpha}$
Thickness (μm)	20	(a) 2, (b) 80, (c) 140
Spin coating cycles	9	(a) 9, (b) 6, (c) 9
Final sintering protocols	0.033 K/s to 1873 K in flowing ambient air and hold for 2 h	(a) 0.033 K/s to 1873 K in flowing ambient air, hold for 2 h and quench to room temperature; (b,c) 0.033 K/s to 1873 K in flowing Ar, hold for 2 h and 0.067 K/s to room temperature and then treatment by ambient air (*air treatment*) at 1273 K for 2 h

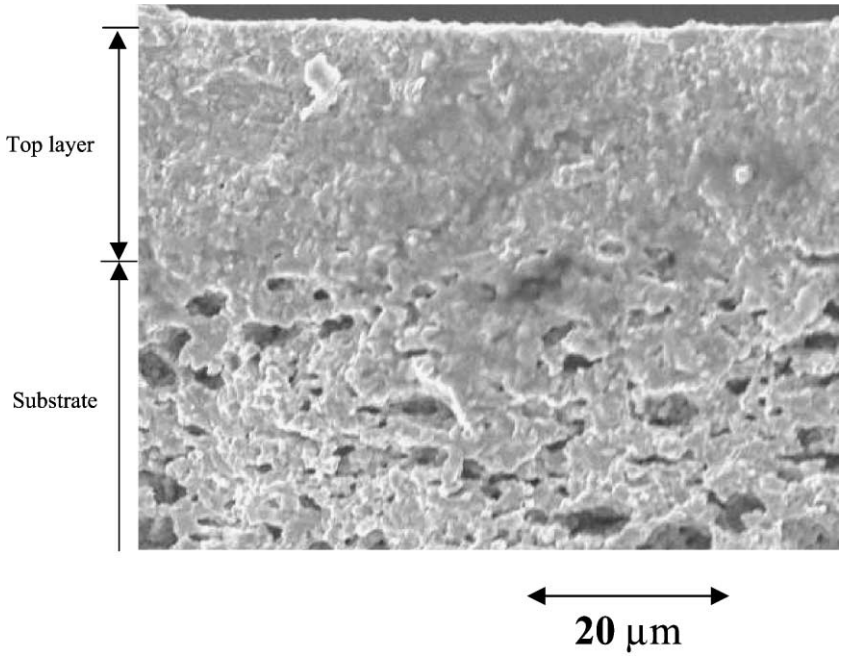

Fig. 5. Scanning electron micrograph of $SrZr_{0.95}Y_{0.05}O_{3-\alpha}$ membrane. Top layer: $SrZr_{0.95}Y_{0.05}O_{3-\alpha}$; substrate: $SrZr_{0.95}Y_{0.05}O_{3-\alpha}$.

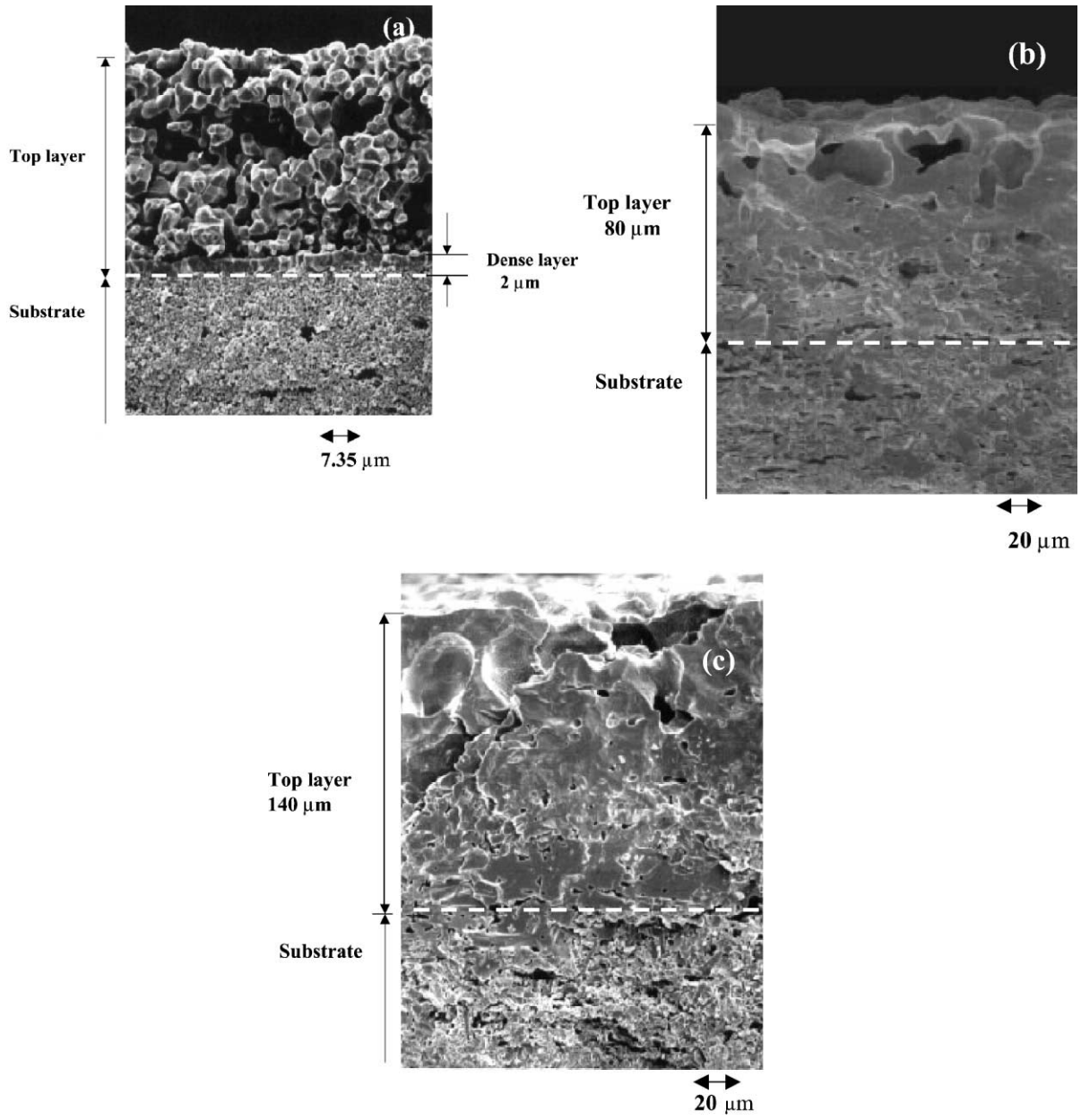

Fig. 6. Scanning electron micrographs of several $SrCe_{0.95}Yb_{0.05}O_{3-\alpha}$ membranes. Top layers: $SrCe_{0.95}Yb_{0.05}O_{3-\alpha}$; substrates: $SrZr_{0.95}Y_{0.05}O_{3-\alpha}$.

ation properties of these materials are likely to reflect the thickness of this thin film, as confirmed by the H_2 permeation data shown in the next section. The reasons for the unusual structure of the material in Fig. 6a remain unclear at this time.

3.3. H_2 permeation rates in $SrCe_{0.95}Yb_{0.05}O_{3-\alpha}$ thin films

The H_2 flux through a 1 mm $SrZr_{0.95}Y_{0.05}O_{3-\alpha}$ disk at 973 K and 200 kPa H_2 was smaller than 10^{-8}

mol/cm^2 min. H_2 transport in this open circuit non-electrochemical mode requires mixed conduction (protons and electrons or holes) and the permeability of one or both of these charge carriers appears to be very low in $SrZr_{0.95}Y_{0.05}O_{3-\alpha}$; as a result, it is not an attractive material for H_2 separations. $SrZr_{0.95}Y_{0.05}O_{3-\alpha}$ materials may be useful, however, as gas sensors or as fuel cell electrolytes, for which only one of the two charge carriers must diffuse, but even as thin films, their permeabilities are too low for accurate measurements.

At similar conditions, the H_2 flux through a 1 mm $SrCe_{0.95}Yb_{0.05}O_{3-\alpha}$ disk is more than 10 times greater than for $SrZr_{0.95}Y_{0.05}O_{3-\alpha}$, making the $SrCe_{0.95}Yb_{0.05}O_{3-\alpha}$ a more attractive choice for the permeation improvements expected by using thin films. Therefore, only H_2 permeation rates on $SrCe_{0.95}Yb_{0.05}O_{3-\alpha}$ films are reported below. Fig. 7 shows H_2 permeation rates at 950 K for $SrCe_{0.95}Yb_{0.05}O_{3-\alpha}$ thin films of varying thickness as a function of H_2 pressure. Permeation rates increased with increasing H_2 pressure and with decreasing thickness of the dense perovskite layer (Fig. 7). The film with a 2 μm dense layer showed a H_2 flux ~ 500 times greater than the 1 mm disk at each H_2 partial pressure. The nonporous nature of the films was confirmed by using N_2 as the diluent in the H_2 stream and ensuring that N_2 concentrations remained below the detection limit in the permeate side.

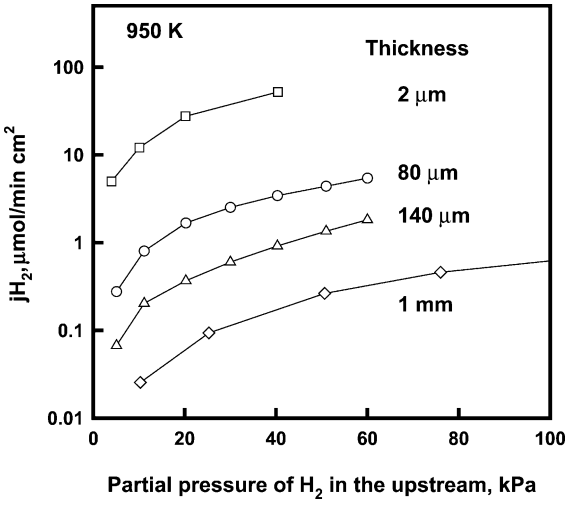

Fig. 7. Comparison of H_2 flux for $SrCe_{0.95}Yb_{0.05}O_{3-\alpha}$ thin films and 1 mm dense disk (950 K).

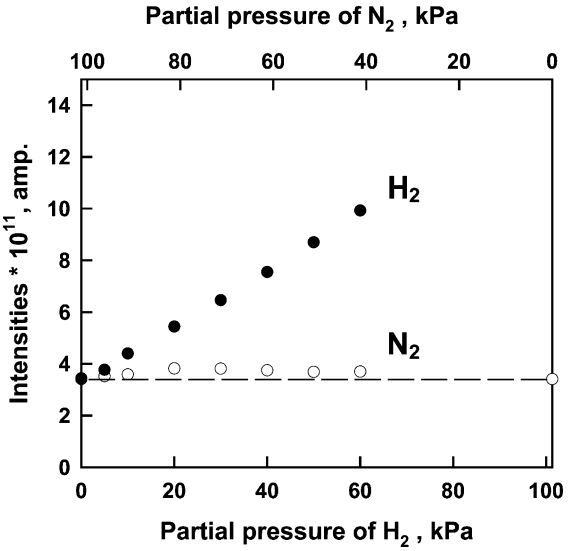

Fig. 8. Changes in the H_2 (2 amu) and N_2 (28 amu) mass spectrometric ion yields in the permeate side with concurrent changes in the H_2 and N_2 partial pressures (0–100 kPa) in the process side (80 μm $SrCe_{0.95}Yb_{0.05}O_{3-\alpha}$ films; 950 K).

Fig. 8 shows the ion yields for H_2 (2 amu) and N_2 (28 amu) in the permeate side of a 80 μm $SrCe_{0.95}Yb_{0.05}O_{3-\alpha}$ film (Fig. 6b) at 950 K as a function of the H_2 and N_2 pressures in the process side. The N_2 signal remains at background levels at all N_2 pressures, indicating the absence of openings large enough for N_2 gas phase transport. The results shown in Fig. 8 are representative of those obtained for the other films, except in those instances in which defective films were formed during synthesis and air treatment. No fissures, cracks, or pores are evident from these data and H_2 permeation appears to occur selectively through the dense perovskite films in all of these samples.

Permeation rates through dense ceramic membranes depend on the mobility of charge carriers in the mixed conductors [6–8]. Occasionally, they also depend on the rate of diffusion of the permeating species through a porous substrate or a gaseous boundary layer and on the rate at which molecules, such as H_2, dissociate at membrane surfaces to form atomic hydrogen. When permeation is not controlled by diffusion through the solid, permeation rates become independent of the

thickness of the dense conductor. This is likely to occur as materials become thinner and total permeation rates increase. In order to clarify the mechanism of hydrogen permeation with mixed conduction in $SrCe_{0.95}Yb_{0.05}O_{3-\alpha}$ thin films, the thickness dependence of the H_2 permeation rates was examined. The dependence of H_2 permeation rates at 950 K and 20 kPa H_2 on membrane thickness is shown in Fig. 9. In previous studies [15–18], permeation rates were found to vary linearly with the reciprocal of the sample thickness for mixed conductors, when permeation was controlled by bulk diffusion. In Fig. 9, hydrogen permeation rates are shown as a function of the reciprocal of the film thickness for the samples in our study. These data show that even for the thinnest films tested, the bulk protonic and electronic conductivities of the dense perovskite films control the H_2 permeation rates through $SrCe_{0.95}Yb_{0.05}O_{3-\alpha}$ thin films at 950 K and 0–60 kPa H_2 partial pressures.

Chen et al. [18] have reported that $La_{0.3}Sr_{0.7}CoO_{3-\alpha}$ mixed oxygen–electronic conductors become limited by adsorption processes for membranes thinner than 80 μm at 1273 K. In our study, 2 μm $SrCe_{0.95}Yb_{0.05}O_{3-\alpha}$ films remained limited by bulk transport. The thickness at which this transition occurs depends on the relative rates of bulk transport and of activation processes at surfaces. Generally, H_2 dissociation is fast on metal oxides than for O_2 dissociation, which often require significant oxygen mobility to generate neighboring vacancies. In addition, proton conductivities in $SrCe_{0.95}Yb_{0.05}O_{3-\alpha}$ at 950 K are much smaller ($\sim 5 \times 10^{-3}$ S cm^{-1} in pure hydrogen [1]) than the oxide ion conductivity in $La_{0.3}Sr_{0.7}CoO_{3-\alpha}$ at 1273 K (0.5 S cm^{-1} in air [18]), and the required electronic conduction is also likely to be smaller in $SrCe_{0.95}Yb_{0.05}O_{3-\alpha}$ at 950 K than in $La_{0.3}Sr_{0.7}CoO_{3-\alpha}$ at 1273 K, leading to lower overall permeation rates via mixed conduction processes. Boundary layer or surface processes are unlikely to control hydrogen permeation of 2 μm $SrCe_{0.95}Yb_{0.05}O_{3-\alpha}$ films at 950 K because of the slow nature of the bulk transport processes through the dense membrane material. This study confirms the limiting step of proton permeation phenomena in $SrCe_{0.95}Yb_{0.05}O_{3-\alpha}$ with a proton and electron mixed conduction at relatively low temperatures (950 K). This assumption was made without direct experimental evidence in previous studies. The results presented show that significant improvements in H_2 permeation rates are possible by decreasing the thickness of mixed proton–electron conductors.

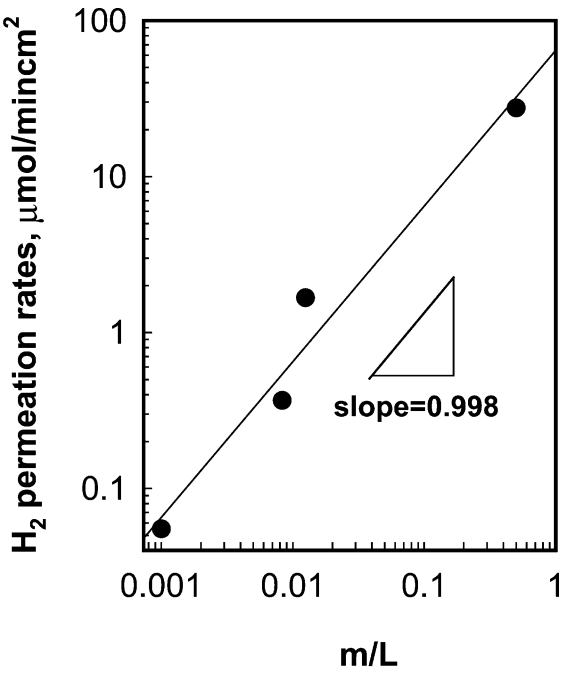

Fig. 9. Thickness dependence of the hydrogen permeation rate of $SrCe_{0.95}Yb_{0.05}O_{3-\alpha}$ thin film (950 K; data from Fig. 7 at a H_2 pressure of 20 kPa).

4. Conclusions

A synthesis procedure to form nonporous $SrZr_{0.95}Y_{0.05}O_{3-\alpha}$ and $SrCe_{0.95}Yb_{0.05}O_{3-\alpha}$ thin films on a porous substrate was developed using spin coating methods. In order to avoid fissures or pinholes, the shrinkage rate of the porous substrate and of the thin film were carefully matched by varying the carbon content, the pre-sintering temperature, and the compaction pressure in carbon–perovskite composites used as precursors for the porous substrates. Undetectable He permeation at ambient temperature and N_2 permeation at 950 K and scanning electron microscopy confirmed the nonporous nature of $SrCe_{0.95}Yb_{0.05}O_{3-\alpha}$ thin films. H_2 permeation rates for 2 μm $SrCe_{0.95}Yb_{0.05}O_{3-\alpha}$ films were more than 100 greater than for 1 mm dense disks of identical composition.

Permeation rates were inversely proportional to the thickness of the dense layers deposited on the porous substrates. This indicates that H_2 permeation rates at 950 K were controlled by bulk diffusion through the dense solids even for 2 μm $SrCe_{0.95}Yb_{0.05}O_{3-\alpha}$ films.

Acknowledgements

Professor Lutgard DeJonghe and Drs. Richard W. Borry, Steve Visco, and Craig Jacobsen are acknowledged for their contributions during the early stages of this project and for their insightful suggestions. Funding was provided by the Federal Energy Technology Center (DOE) (Contract DE-AC03-76SF00098) under the supervision of Dr. Daniel J. Driscoll. One of the authors (S.H.) acknowledges the financial support from Ministry of Education, Culture, Sports, Science and Technology (MEXT) of Japan for a 1-year stay at the University of California at Berkeley.

References

[1] H. Iwahara, Solid State Ionics 86–88 (1996) 9–15.
[2] A.S. Nowick, Y. Du, Solid State Ionics 77 (1996) 137–146.
[3] K.D. Kreuer, Solid State Ionics 97 (1997) 1–15.
[4] K.D. Kreuer, Solid State Ionics 125 (1999) 285–302.
[5] T. Norby, Solid State Ionics 125 (1996) 1–11.
[6] S. Hamakawa, T. Hibino, H. Iwahara, J. Electrochem. Soc. 141 (1994) 1720–1725.
[7] X. Qi, Y.S. Lin, Solid State Ionics 130 (2000) 149–156.
[8] H.J.M. Bouwmeester, A.J. Burggraaf, in: A.J. Burggraaf, L. Cot (Eds.), Fundamentals of Inorganic Membrane Science and Technology, Elsevier, Amsterdam, 1996, Chapter 10.
[9] H. Itoh, H. Asano, K. Fukuroi, M. Nagata, H. Iwahara, J. Am. Ceram. Soc. 80 (1997) 1359.
[10] S.J. Visco, L.S. Wang, S. Souza, L.C. De Jonghe, Mater. Res. Soc. Symp. Proc. 369 (1995) 683.
[11] J. Eschenbaum, J. Rosenberger, R. Hempelmann, D. Nagengast, A. Weidinger, Solid State Ionics 77 (1995) 222.
[12] I. Kosacki, H.U. Anderson, Solid State Ionics 97 (1997) 429.
[13] E.C. Lu, E. Iglesia, J. Mater. Sci. 36 (2001) 77.
[14] M.N. Rahaman, Ceramic Processing and Sintering, Marcel Dekker, New York, 1995.
[15] X. Tan, S. Liu, K. Li, R. Hughes, Solid State Ionics 138 (2000) 149–159.
[16] T. Norbby, Y. Larring, Solid State Ionics 136–137 (2000) 139–148.
[17] L. Li, S. Hamakawa, E. Iglesia, Chem. Eng. Sci., in preparation.
[18] C.H. Chen, H.J.M. Bouwmeester, R.H.E. van Doorn, H. Kruidhof, A.J. Burggraaf, Solid State Ionics 98 (1997) 7–13.